Rev.Adv.Mater.Sci. 18(2008) 464-468

STUDY OF CRYSTALLIZATION PROCESS OF $Fe_{65}Nb_{10}B_{25}$ AND $Fe_{70}Nb_{10}B_{20}$ GLASSY METALS

J. Torrens-Serra[1] , P. Bruna[2], J. Rodríguez-Viejo[1], T. Pradell[3] and M.T. Clavaguera-Mora[1]

[1]Departament de Física, Universitat Autónóma de Barcelona, Edifici Cc, 08193 Bellaterra, Spain
[2]Dept. de Física Aplicada, Escola Politècnica Superior de Castelldefels, Universitat Politècnica de Catalunya, Avda. del Canal Olímpic s/n, 08860-Castelldefels, Spain
[3]Dept. de Física i Enginyeria Nuclear, Escola Superior d'Agricultura de Barcelona, Universitat Politčcnica de Catalunya, Avda. del Canal Olímpic s/n, 08860-Castelldefels, Spain

Received: March 29, 2008

Abstract. The devitrification of the $Fe_{65}Nb_{10}B_{25}$ and $Fe_{70}Nb_{10}B_{20}$ metallic glasses produced by melt spinning has been studied by calorimetry (DSC), X-ray diffraction (XRD) and transmission Mössbauer spectroscopy (TMS). Calorimetric measurements show three exothermic peaks which have been identified as the successive primary nanocrystallization of mainly a $Fe_{23}B_6$-type phase, the formation of bcc-Fe and metastable borides and finally the transformation to the stable phases. TMS and XRD have been used to identify and follow the evolution of the phases that appear in the different transformations.

1. INTRODUCTION

The Fe-TM-B (TM=Nb,Zr,Hf) amorphous and nanocrystalline alloys have been widely studied during the last decade due to the promising properties to be used for soft magnetic applications [1-5]. The properties required are large saturation magnetization, low coercive field and high permeability. These properties are obtained by a partial crystallization of the amorphous alloy as a consequence of a heat treatment [4]. In addition, good thermal properties as wide supercooled liquid range and phase stability until high temperatures are needed to bulk metallic glasses. For that purpose, studies of alloys with higher content of boron and niobium have been done [6-8]. The stability of nanocrystalline alloys is attributed to the formation of a diffusion barrier around the nanocrystals formed by heavy atoms that can not diffuse to the amorphous matrix. In this work we present a study of the devitrification process of $Fe_{65}Nb_{10}B_{25}$ and $Fe_{70}Nb_{10}B_{20}$ amorphous alloys and the formation of the diffusion barrier during primary crystallization by means of different techniques.

2. EXPERIMENTAL PROCEDURE

Glassy $Fe_{65}Nb_{10}B_{25}$ and $Fe_{70}Nb_{10}B_{20}$ (labeled Fe65 and Fe70, respectively) ribbons were prepared by melt spinning under Ar atmosphere with single Cu roller at a linear velocity of about 40 m/s. The ingots were prepared from Fe, Fe_2B (98% purity) and NbB (99% purity) powders, pressed at 150 kg/cm^2 and melted for 15 s in an induction furnace to improve homogeneity. The ribbons are about 20 μm thick and 2 mm wide. The as-prepared and annealed samples were examined by XRD in a Philips X'Pert diffractometer using CuK_α radiation in a wide angle.

Calorimetric measurements have been performed in a NETZSCH DSC404 differential scanning calorimeter under dynamic pure argon atmo-

Corresponding author: J. Torrens-Serra, e-mail: joan@vega.uab.es

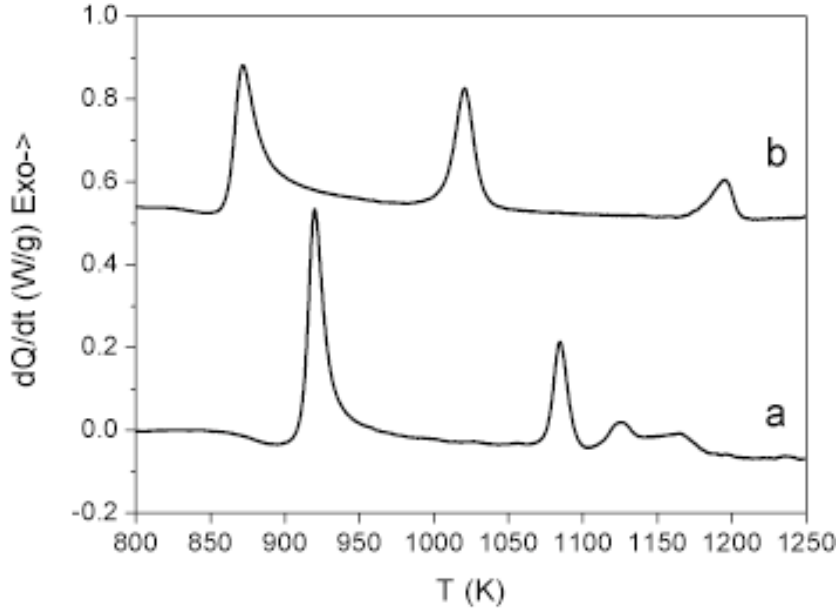

Fig. 1. DSC scans for alloys (a) Fe65 and (b) Fe70 at 10 K/min.

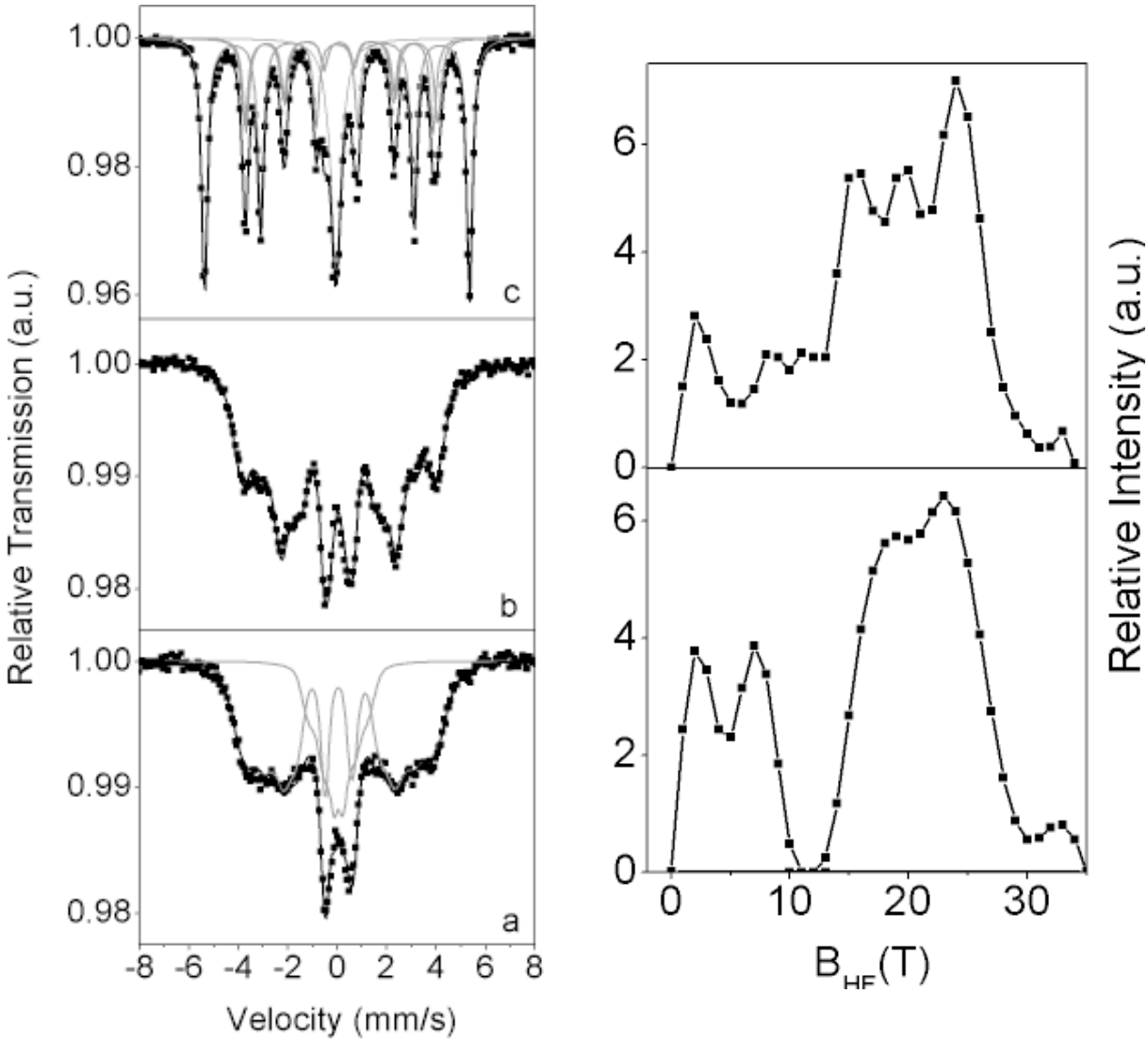

Fig. 2. Left: experimental TMS spectra (dots) and fittings (in grey each subspectra and in black the total fitting). Right: the corresponding hyperfine field distribution for alloy Fe65 heated up at 10 K/min to (a) 998K, (b) 1103K, and (c) 1273K.

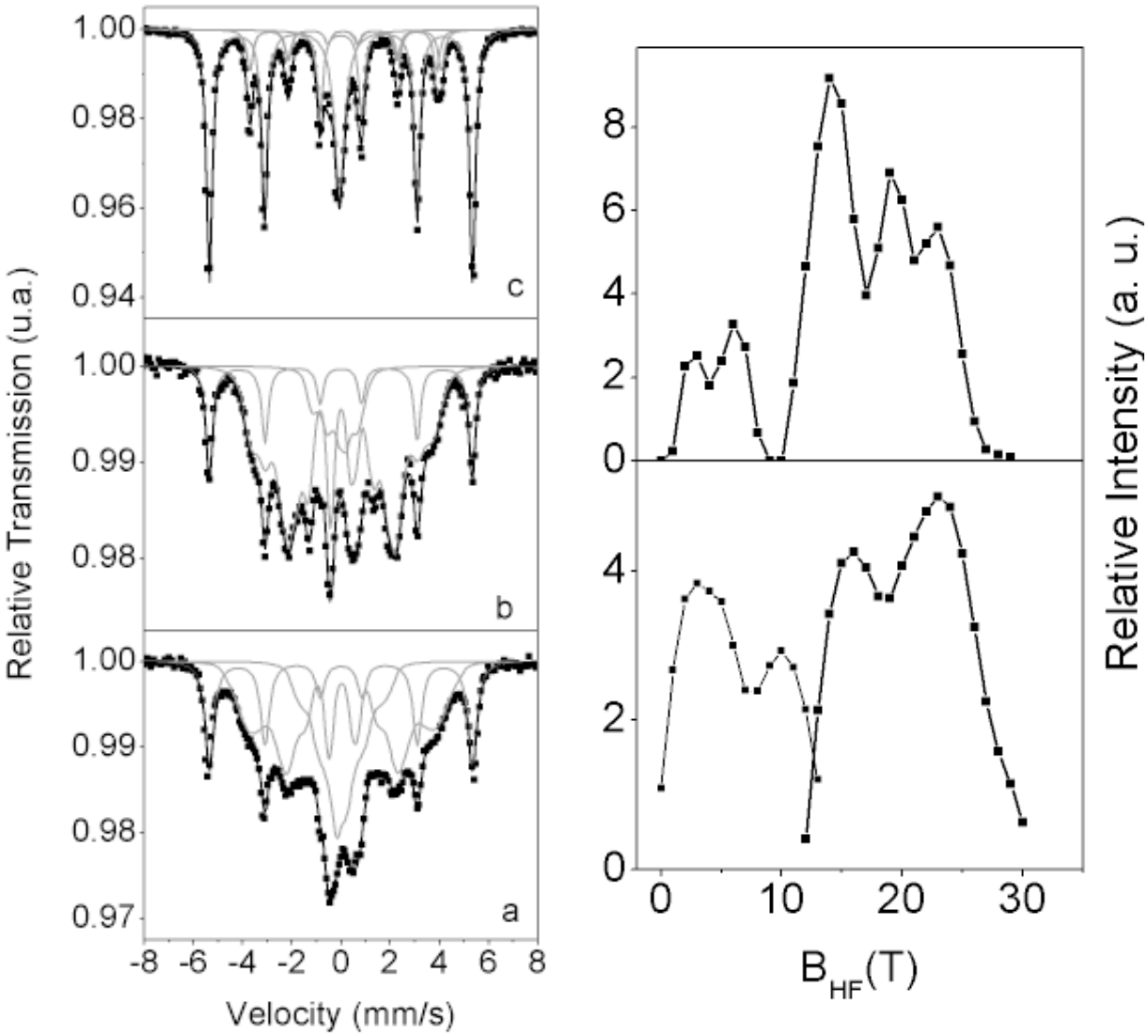

Fig. 3. Left: experimental TMS spectra (dots) and fittings (in grey each subspectra and in black the total fitting). Right: the corresponding hyperfine field distribution for alloy Fe70 heated up at 10 K/min to (a) 998K, (b) 1103K, and (c) 1273K.

sphere. A second scan has been always done in order to subtract the DSC baseline. Room temperature transmission Mössbauer spectra were obtained using a conventional constant acceleration spectrometer with a 25 mCi source of ^{57}Co in Rh matrix. Experimental spectra were fitted with Brand's NORMOS program [9], considering one or two histogram magnetic hyperfine-field distributions with linear correlation between the isomer shift and the magnetic field. The isomer shift values are given relative to room temperature bcc-Fe.

3. RESULTS AND DISCUSSION

The XRD and TMS spectra of the melt spun Fe65 and Fe70 alloys show the characteristic pattern for a glass. The TMS spectra have been fitted with one magnetic hyperfine field distribution, with average values of 9.86(3) T for Fe65 and 9.8(2) T for Fe70. The devitrification process in both metallic glasses occurs in three different stages (Fig. 1). The glass transition precedes the three exothermic peaks observed in the DSC curves when heating the alloys up to 1273K. As shown by XRD, the

Table 1. Hyperfine parameters for both ribbons. In all the cases the A13 and A23 quotients are close to 3 and 2 respectively.

T(K)		*IS* (mm/s)		*QS* (mm/s)		*HF* (T)	
		Fe 65	Fe 70	Fe 65	Fe 70	Fe 65	Fe 70
melt spun		0.00 (1)	-0.03 (2)	0.006 (2)	-0.02 (1)	9.86 (3)	9.8 (2)
998	Nb-poor	0.05 (2)	0.04 (2)	0.009 (6)	0.003 (9)	21.7 (1)	20.56 (6)
	Nb-rich	0.03 (2)	0.00 (2)	-0.03 (1)	0.04 (2)	5.01 (9)	6.13 (5)
	Alpha-Fe		-0.001 (2)	-0.007 (3)		33.1	33.1
1103	Nb-poor	0.04 (2)	-0.106 (5)	0.015 (5)	-0.24 (2)	17.71 (2)	17.82 (2)
	Nb-rich		0.01 (4)		-0.026 (5)		4.76 (3)
	Alpha-Fe		-0.007 (3)		-0.003 (5)	33.1	33.1
1273	FeNbB	-0.066 (2)	-0.064 (1)	-	-	-	-
	Fe_2B	0.083 (6)	0.072 (8)	0.02	0.02	23.46 (4)	23.52 (7)
		0.124 (7)	0.132 (9)	0.070 (7)	0.081 (6)	24.22 (5)	24.16 (6)
	Alpha-Fe	-0.007 (1)	-0.0093 (4)	0.001 (2)	0.0070 (8)	33.226 (7)	33.1

first DSC peak corresponds to the nanocrystallization in both alloys [10]. The peak onset is sharp but the last part of the decay occurs in a wide temperature interval. That effect is more pronounced in sample Fe70 than in Fe65. Such a tail in the DSC signal is often observed in primary nanocrystallization processes due to soft impingement [11]. The TMS spectrum of sample Fe65, once nanocrystallized (Fig. 2), has been fitted using two magnetic hyperfine field (high and low) distributions. Low field one presents two maxima (at 2 T and 7 T) attributed to a Nb-rich environment amorphous phase. The high field distribution has three maxima (at 18 T, 24 T, and 33 T) which are attributed, respectively, to the presence of a Fe-B environment, a $Fe_{23}B_6$-type phase [12,13] and a small amount of bcc-Fe. For the nanocrystallized Fe70 sample, similar results are found from the analysis of the TMS spectra (see Fig 3), but an extra sextet corresponding to bcc-Fe has been added to the fit. The values of the hyperfine field (HF) as well as the isomer shift (IS) and quadrupole splitting (QS) parameters can be seen in Table 1. The relative area shows that the relative amount of bcc-Fe increases from 5.6% for Fe65 to 22.8% for Fe70 in detriment of the Fe-B environment. The assignment of crystalline phases agrees with the measured XRD patterns [10,14].

These results indicate that, apart from the $Fe_{23}B_6$-type and bcc-Fe nanocrystals, two distinct disordered type of environments, being respectively rich and poor in Nb, exist in the nanocrystallized samples. The Nb-rich disordered phase was probably produced by the expulsion of Nb out of nanocrystals and surrounds the $Fe_{23}B_6$ and bcc-Fe nanocrystals, acting as a diffusion barrier limiting crystal growth. The Nb-poor disordered phase corresponds most probably to the remaining disordered matrix.

The XRD and TMS spectra obtained for samples heated up to the end of the second crystallization peak indicate the presence of Fe_3B-orthorhombic boride [15], coexisting with bcc-Fe, in both alloys. The TMS spectra of fully crystalline samples (1273K) has been fitted with three sextets, two corresponding to Fe_2B and one to bcc-Fe, and a singlet for the FeNbB paramagnetic phase. The quantification obtained by TMS shows an increase of the bcc-Fe/Fe_2B ratio with the iron content of the alloy (from 1.37 to 2.89) and a virtually constant percentage of FeNbB (18.21% for Fe65 and 17.20% for Fe70). Consequently, the decomposition of the metastable borides and the transformation of the remaining amorphous phase in the last transformation results in the stable phases, bcc-Fe, Fe_2B and FeNbB, the last one resulting mainly from the transformation of the Nb-rich environments.

4. CONCLUSIONS

The slow down during the nanocrystallization process of $Fe_{65}Nb_{10}B_{25}$ and $Fe_{70}Nb_{10}B_{20}$ amorphous

alloys is associated to the formation of a Nb-rich disordered phase surrounding the $Fe_{23}B_6$ and bcc-Fe nanocrystals, acting as a diffusion barrier.

The addition of a high percentage of Nb to Fe-B amorphous alloys promotes their devitrification by the precipitation of a $Fe_{23}B_6$-type phase and shifts the appearance of the metastable Fe_3B phase to higher temperatures.

ACKNOWLEDGEMENTS

Authors want to thank Dr. S. Roth and the IFW-Dresden for calorimetric measurements facilities. This work was financed by Generalitat de Catalunya through project 2005SGR00201 and the Spanish ministry of science and technology under projects MAT2003-8271-C02, MAT2004-01214, and MAT2007-61521. J.T-S. acknowledges the MEC predoctoral grant.

REFERENCES

[1] A. Makino, T. Hatanai, A. Inoue and T. Masumoto // *Mater. Sci. Eng A* **226-228** (1997) 594.

[2] A. Makino, K. Suzuki, A. Inoue and T. Masumoto // *Mater. Sci. Eng. A* **179/180** (1994) 127.

[3] Y. Naitoh, T. Bitoh, T. Hatanai, A. Makino, A. Inoue and T. Masumoto // *Nanostructured Mater.* **8** (1997) 987.

[4] M.E. McHenry, M.A.Willard and D.E. Laughlin // *Prog. Mater. Sci.* **44** (1999) 291.

[5] K. Suzuki, J.M. Cardogan, V. Sahajwalla, A. Inoue and T. Masumoto // *Mater. Sci. Eng. A* **226-228** (1997) 554.

[6] M. Imafuku, S. Sato, H. Koshiba, E. Matsubara and A. Inoue // *Scripta Mater.* **44** (2001) 2369.

[7] B. Yao, L. Si, H. Tan, Y. Zhang and Y. Li // *J. Non-Cryst. Solids* **332** (2003) 43.

[8] M. Shapaan, J. Lábár, L. Lendvai and L. K. Varga // *Mater. Sci. Eng. A* **375-377** (2004) 789.

[9] R. Brand, J. Lauer and D. Herlach // *J.Phys. F.: Metal. Phys.* **14** (1984) 555

[10] J. Torrens-Serra, J. Rodríguez-Viejo and M.T. Clavaguera-Mora // *J. Non-Cryst. Solids* **353** (2007) 842.

[11] M.T. Clavaguera-Mora, N. Clavaguera, D. Crespo and T. Pradell // *Prog. Mater. Sci.* **47** (2002) 559.

[12] P. Gorria, J.S. Garitaonandia and J.M. Barandiarán // *J.Phys.: Condens. Matter.* **8** (1996) 5925.

[13] M.T. Raposo, J.D. Ardisson, A.I.C. Persiano and R.A. Mansur // *Hyperfine Interact.* **83** (1994) 235.

[14] J. Torrens-Serra, P. Bruna, J. Rodríguez-Viejo, M.T. Clavaguera-Mora and T. Pradell // *AIP Conference proceedings* **765** (2005) 250.

[15] F.H.Sanchez, J.I. Budnick, Y.D. Zhang, W.A. Hines, M. Choi and R. Hasegawa // *Physical Review B* **34** (1986) 4738.